ResearchGate

See discussions, stats, and author profiles for this publication at: https://www.researchgate.net/publication/231231186

Epitaxial Growth of Au@Cu Core–Shell Nanocrystals Prepared Using the PVP-Assisted Polyol Reduction Method

ARTICLE *in* CRYSTAL GROWTH & DESIGN · DECEMBER 2010

Impact Factor: 4.89 · DOI: 10.1021/cg100860d

CITATIONS
34

READS
36

4 AUTHORS, INCLUDING:

Masaharu Tsuji
Kyushu University
442 PUBLICATIONS **6,291** CITATIONS
SEE PROFILE

Jahangir Alam
University of Rajshahi
10 PUBLICATIONS **91** CITATIONS
SEE PROFILE

Available from: Masaharu Tsuji
Retrieved on: 03 February 2016

DOI: 10.1021/cg100860d

CRYSTAL GROWTH & DESIGN Article

2010, Vol. 10
5129–5135

Epitaxial Growth of Au@Cu Core−Shell Nanocrystals Prepared Using the PVP-Assisted Polyol Reduction Method

Masaharu Tsuji,*[,†,‡] Daiki Yamaguchi,[‡] Mika Matsunaga,[†] and Md. Jahangir Alam[‡]

[†]*Institute for Materials Chemistry and Engineering, Kyushu University, Kasuga 816-8580, Japan, and* [‡]*Department of Applied Science for Electronics and Materials, Graduate School of Engineering Sciences, Kyushu University, Kasuga 816-8580, Japan*

Received June 29, 2010; Revised Manuscript Received October 13, 2010

ABSTRACT: Au@Cu core−shell nanocrystals were prepared using a two-step polyol reduction method. First, mixtures of octahedral, triangular and hexagonal platelike, decahedral, and icosahedral Au core seeds were prepared by reducing $HAuCl_4 \cdot 4H_2O$ in ethylene glycol (EG) using microwave (MW) heating in the presence of polyvinylpyrrolidone (PVP) as a polymer surfactant. Then Cu shells were overgrown on Au core seeds by reducing $Cu_2(OAc)_4$ in EG with PVP using oil-bath heating. Resultant crystal structures were characterized using TEM, high-resolution (HR)-TEM, TEM-EDS, and selected area electron diffraction (SAED) measurements. A large mismatch exists in lattice constants between Au (0.4079 nm) and Cu (0.3615 nm). No monometallic Cu nanocrystals having well-defined facets were prepared by reducing $Cu_2(OAc)_4$ in EG. Therefore, the epitaxial growth of Cu shells over Au cores was expected to be difficult. Nevertheless, flat {111} facets of Cu shells were grown epitaxially on {111} facets of Au cores. The SAED patterns and Moiré patterns showed Cu layers parallel to Au layers. The Cu shell growth on sharp Au-core corners was slower than that on flat {111} facets and single twin facets. This report is the first describing epitaxial growth of core−shell nanocrystals despite a large lattice mismatch (11.4%). The Au@Cu nanoparticles were more antioxidative than pure Cu particles prepared under identical conditions.

Introduction

In recent years, bimetallic nanoparticles have received intensive attention because of their novel optical, electronic, magnetic, and catalytic properties, which differ from those of their respective constituent metals.[1−17] We have recently studied shape-selective growth of Au@Ag core−shell nanocrystals prepared using a two-step method.[18−20] First, Au nanocrystal seeds of various shapes including single-crystal octahedron, single-twinned triangular or hexagonal plate, and multiple-twinned decahedron were prepared by reducing $HAuCl_4$ in ethylene glycol (EG) in the presence of polyvinylpyrrolidone (PVP) as a polymer surfactant under microwave (MW) heating. Although these Au nanoparticles have different shapes, a common feature is that they are mainly surrounded by {111}-type facets. Subsequently, the obtained Au seeds were added to either EG or *N*,*N*-dimethylformamide (DMF) solution for overgrowth of Ag shells by MW heating or oil-bath heating. Here EG and DMF act as both a solvent and a reductant. Transmission electron microscopic (TEM) and TEM-energy dispersed X-ray spectroscopic (EDS) observations revealed that the shapes of Ag shells depend strongly on both the shapes of Au seeds and the solvent/reductant. Cubic, triangular-bipyramidal, and rod/wire Ag shells with {100}-type dominant facets were formed epitaxially over octahedral, triangular platelike, and decahedral Au core seeds in EG, respectively, whereas the same shapes as those of Au cores with {111}-type facets were overgrown on Au core seeds in DMF. Our results demonstrated the possibility of preparing the Au@Ag core/shell nanocrystal structures controllably with optional uniform crystalline planes using the same Au seed source and different reaction solvent and reductant because of the negligibly small lattice mismatch (0.2%) between Au (lattice constant: 0.4079 nm) and Ag (0.4086).

Recently, Fan et al.[7] reported a simple and effective route to synthesize bimetallic core−shell nanocubes in aqueous solution using a two-step seed-mediated growth method with Au nanooctahedra as cores. Their systematic investigation of the growth of core−shell heterogeneous structures of four typical noble metals (i.e., Au, Ag, Pd, and Pt) revealed the relevant growth modes and general criteria for the conformal epitaxial growth or the heterogeneous nucleation and growth of various noble metals. They found that two different forms exist for the growth of heterogeneous metal shells on the gold core: the conformal epitaxial growth for Au@Pd and Au@Ag nanocubes, and the heterogeneous nucleation and island growth for Au@Pt nanospheres. Based on results of their systematic studies, they proposed the following rules for the epitaxial layered growth of heterogeneous core−shell nanocrystals. (i) The lattice constants of two metals are expected to be comparable, with lattice mismatch of less than about 5%. The shell metal with the smaller atomic radius is easier to grow epitaxially on the core because it can uniformly release the lattice strain resulting from the lattice mismatch. (ii) The electronegativity of the shell metal should be lower than that of the core metal to avoid the displacement reaction and to wet the surface of the core easily. (iii) The bond energy between metal atoms of the shell should be smaller than that between the shell atoms and substrate atoms to ensure growth in the Frank−van der Merwe mode. Only three core−shell structures (Pt@Pd, Au@Pd, and Au@Ag) can well meet the three rules described above, which show good agreement with their experimental results. The epitaxial growth of Pt@Pd, Au@Pd, and Au@Ag nanocrystals has also been observed in other studies.[4−6,8,9]

Compared with a number of studies on the epitaxial growth of bimetallic particles between novel metals, little work has

*To whom correspondence should be addressed: E-mail: tsuji@cm.kyushu-u.ac.jp.

© 2010 American Chemical Society

Published on Web 11/02/2010

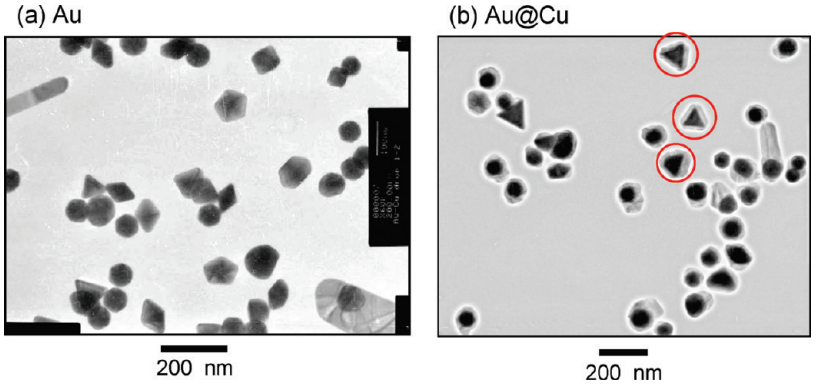

Figure 1. TEM images of (a) Au core and (b) Au@Cu nanocrystals prepared using the polyol method.

been reported on the epitaxial growth of bimetallic metals between novel metals and transition metals such as Ni, Co, and Cu. For example, cobalt has a smaller atomic radius than copper and has been adopted as the shell metal for Pt@Co, Au@Co, and Ag@Co core−shell structures.[15−17] However, epitaxial growth in the Frank−van der Merwe mode has not been reported for these three core−shell particles.

In this study, we investigate the preparation of Au@Cu nanocrystals using a two-step method resembling that used for the epitaxial growth of Au@Ag nanocrystals.[18−20] On the basis of TEM, HR-TEM, TEM-EDS, and SAED data, crystal structures of products and their growth mechanisms are examined. The effects of lattice mismatch between core and shell atoms are investigated. These results show for the first time that Cu shells can be formed epitaxially on Au cores despite a large lattice mismatch between Au and Cu (11.4%). These results also show that the epitaxial growth rate of Cu layers depends strongly on the positions of cores, e.g., flat planes or sharp corners. Moreover, Au@Cu nanocrystals have a higher antioxidative property than that of monometallic Cu particles.

Experimental Section

For use in this study, $HAuCl_4 \cdot 4H_2O$ (>99.0%), EG (>99.5%), $Cu_2(OAc)_4$ (>99.0%), and C_2H_5OH (>99.5%) were purchased from Kishida Chemical Industry Ltd., and PVP (M_w = 40k in terms of monomeric units) and PVP (M_w = 55k) were obtained from Wako Pure Chemical Industries Ltd. and Sigma-Aldrich Corp., respectively. All reagents were used without further purification.

For this study, Au@Cu core−shell nanocrystals were prepared using a two-step reduction method. In our experiments, EG was used as both a reductant and solvent. As the first step, Au nanocrystal seeds were prepared by MW heating in EG. In the process, 2.4 mM of $HAuCl_4 \cdot 4H_2O$ was dissolved in 20 mL of EG solvent. Then, 1 M PVP (M_w = 40k) was added to the solution above. The whole reaction system was heated for 3 min using MW irradiation in a continuous wave mode (μ Reactor, 500 W; Shikoku Keisoku Kogyo K.K.). The solution temperature increased to 198 °C after heating for about 1.5 min; it was kept at this temperature for about 1.5 min. After natural cooling to room temperature, the Au seeds were separated from C_2H_5OH solution by centrifuging the colloidal solution three times at 15,000 rpm for 30 min. Then it was redispersed in a 3 mL EG solution to prepare an 8 mM Au seed solution. In the second step, 14 mL of EG solution containing 249 mM PVP (M_w = 55k) was preheated at 175 °C for 10 min under bubbling Ar gas at a flow rate of 150 mL/min. Subsequently, Au seeds in 3 mL of EG solution were added to the solution described above. Then, 24 mM $Cu_2(OAc)_4$ in 3 mL of EG solution was injected dropwise to the solution using a syringe pump at an injection rate of 0.3 mL/min. The final concentrations of Au, Cu, and PVP were 1.2, 3.6, and 211 mM, respectively. After all reagents were introduced to the solution, the solution was heated in the oil-bath for 5 min. Then the total heating time after injection of $Cu_2(OAc)_4$ was 15 min. For comparison, Cu nanoparticles were prepared in EG in the presence of PVP under oil-bath heating or MW heating.

The Au@Cu and Cu particles were obtained from C_2H_5OH solution by centrifuging the colloidal solution at 15,000 rpm for 30 min three times for TEM (JEM-2000XS; JEOL) observations. The HR-TEM and TEM-EDS data were also measured (2100F; JEOL). X-ray photoelectron spectra (XPS) of Au@Cu on a Si substrate were measured to characterize product surfaces (JPS-9010MC/IV; JEOL). Extinction spectra of the product solutions were measured in the ultraviolet (UV)−visible (vis)−near infrared (NIR) region using a spectrometer (UV-3600; Shimadzu Corp.).

Results and Discussion

Preparation of Au@Cu Nanocrystals and Their Crystal Structures. Our previous study revealed that mixtures of polygonal nanocrystals can be prepared rapidly under MW heating of $HAuCl_4$/PVP(40k)/EG solution.[21] We used similar MW heating for the synthesis of mixtures of Au nanocrystals of various shapes to examine effects of crystal shapes of Au seeds in the formation of Au@Cu nanocrystals. Figure 1a portrays a typical TEM image of Au nanocrystals prepared under MW heating, where a mixture of octahedral, triangular-platelike, decahedral, and icosahedral Au nanocrystals was observed. As explained later, octahedral particles are single-crystal, triangular-platelike particles are single-twin particles, and decahedral and icosahedral particles are multiple-twin particles. All of these seed particles have {111} facets as major planes.

The Au@Cu particles were prepared by dropwise injection of $Cu_2(OAC)_4$/EG solution to an Au seeds/PVP(55k)/EG solution preheated to 175 °C under bubbling Ar gas. A typical TEM image of product particles is portrayed in Figure 1b. In most product particles, dark contrast polygonal Au cores are covered by light contrast Cu shells. It is noteworthy that triangular Au cores are covered by thin triangular Cu shells, as indicated by red circles.

To confirm the formation of Au@Cu core−shell structures, TEM-EDS measurements were conducted (Figure 2). The data clarify that Au core components having various shapes are covered by Cu shell components; these data also confirm that no Au/Cu alloy exists in the products. The TEM-EDS data demonstrate that triangular Au cores are covered by the same shapes of triangular Cu shells, which implies that the favorable facets of Cu shells are {111}, as in the case of Au cores, so that triangular shapes of Au cores are reserved in Cu shells. Figure 3a presents a typical expanded TEM-EDS image of a triangular Au@Cu plate. Figure 3b

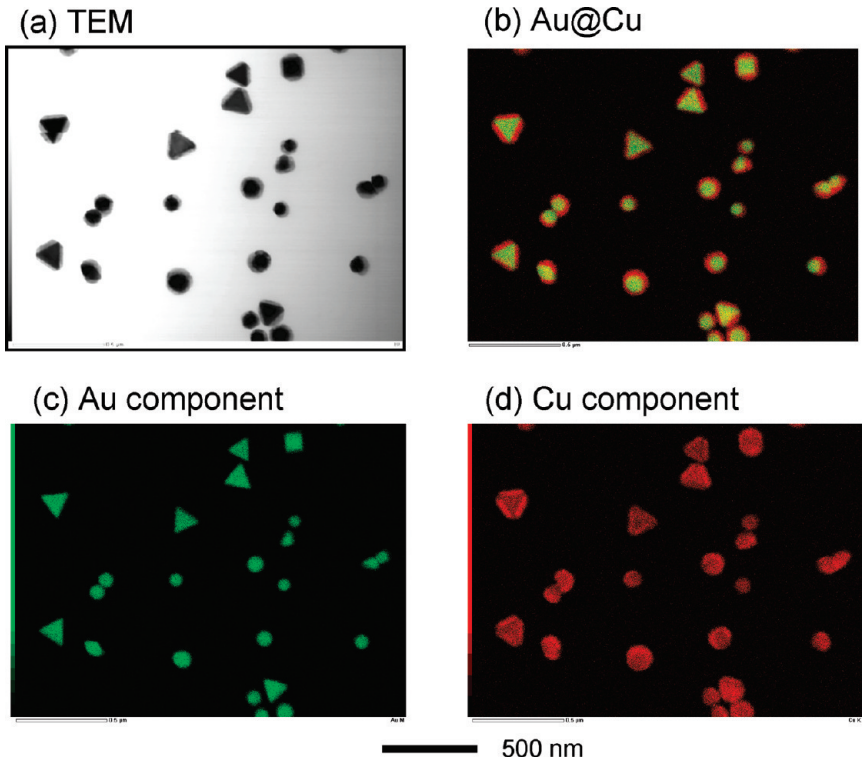

Figure 2. (a) TEM and (b−d) TEM-EDS data of Au@Cu nanocrystals prepared from an Au seeds/$Cu_2(OAc)_4$/PVP(55k)/EG mixture using oil-bath heating.

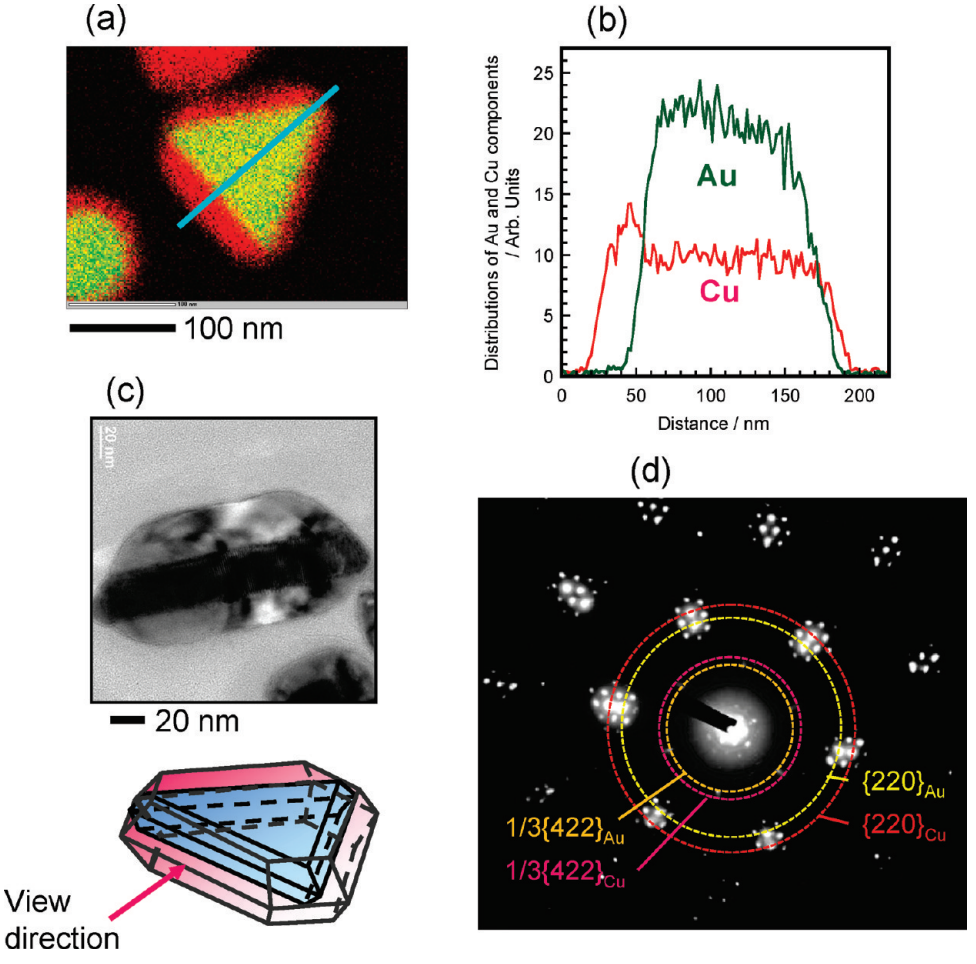

Figure 3. (a) EDS; (b) line analysis along the line in part a; (c) side view of TEM; (d) SAED pattern of platelike Au@Cu nanocrystals.

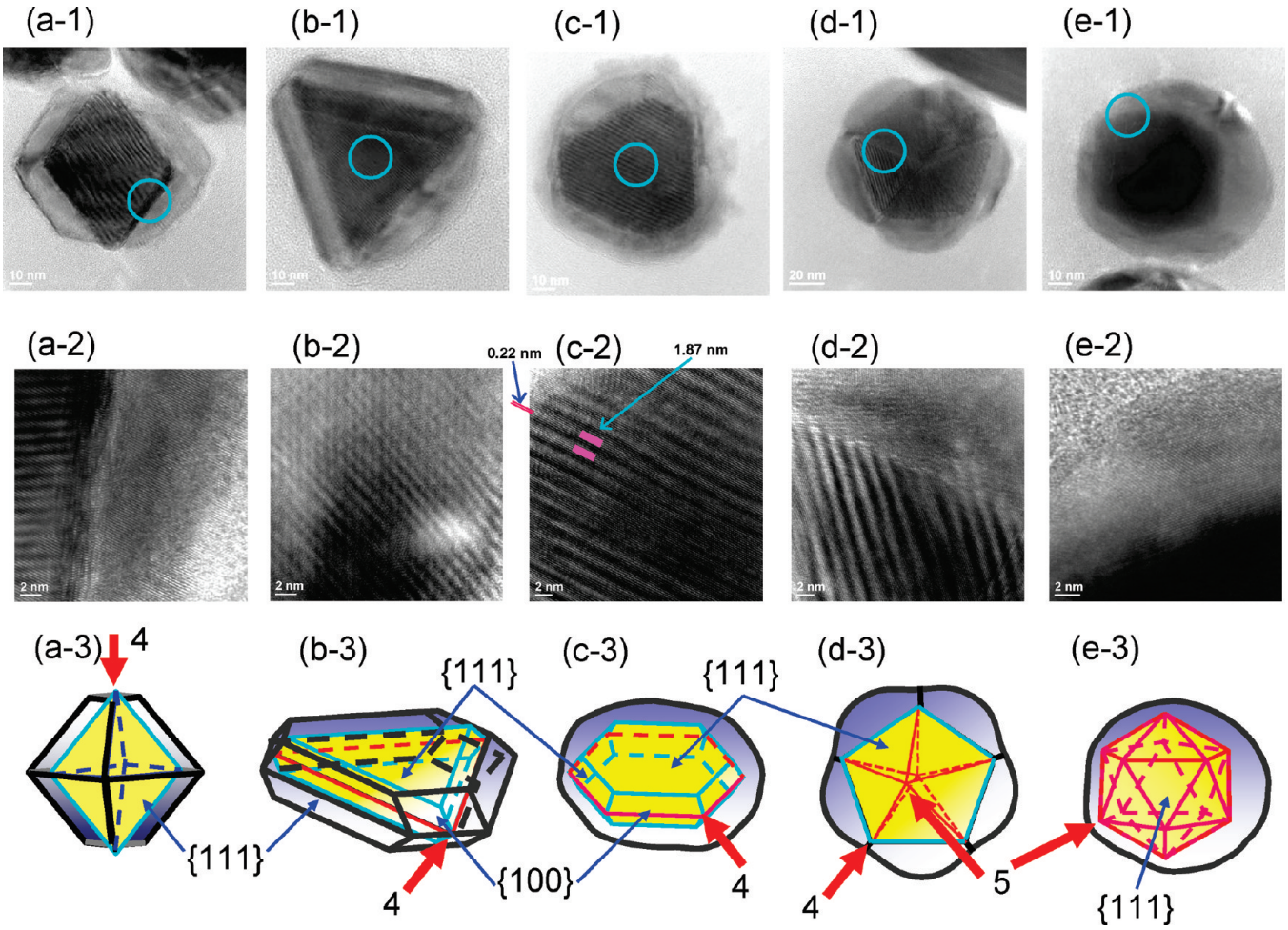

Figure 4. HR-TEM images of Au@Cu nanocrystals having various Au cores, along with their crystal structures. The blue circles in parts a-1 to e-1 are expanded respectively in parts a-2 to e-2. The red lines in parts a-3 to e-3 are twin planes in Au cores. The red arrows in parts a-3 to e-3 are corners in which more than four facets mutually intersect. For the sake of clarity, only typical positions are indicated by red arrows; the number 4 or 5 represents the total number of facets located on each corner.

displays distributions of Au and Cu components along a diagonal line in Figure 3a. The distribution of a triangular Au twin-plate is flat in the center parts, decreasing at a side edge or corner. The distribution of Cu has a maximum at the edge, is flat on the plane, and decreases greatly on a side edge or corner. Similar distributions between Au and Cu components indicate that the Cu shell has a similar platelike structure. This finding is consistent with a side view of a typical triangular plate (Figure 3c), where a single-twin Au plate is covered by the two upper and lower Cu plates.

Selected area electron diffraction (SAED) patterns were measured by focusing the electron beam perpendicularly on the flat surface of the nanoplates. Figure 3d portrays a typical SAED pattern from the plate sample. It exhibits two sets of hexagonal symmetry patterns in which six heavy black spots corresponding to the {220} reflections of the faced-centered-cubic (fcc) Au and Cu single-crystal orientated in the [111] direction are observed, strongly suggesting that the flat surfaces of the nanoplates are parallel to the {111} plane. Furthermore, a set of weaker spots at the positions of 1/3{422} has been found, indicating a twinning boundary within the Au {111} and Cu {111} planes normal to the TEM electron beam. The 1/3{422} reflections are thought to be forbidden for a perfect fcc single-crystalline structure.[19,22] In addition to hexagonal spots, small hexagonal double-diffraction spots are observed around the {220} spots of Au and Cu. Some of the double-diffraction spots of Au and Cu are partially superimposed with each other. It is noteworthy that the same SAED patterns attributable to Au and Cu, partially overlapping, are observed on the same lines from the center of the diffraction pattern, including double-diffraction spots. These results led us to conclude that Cu {111} facets are grown epitaxially on Au {111} facets despite the presence of a large lattice mismatch between Au (0.4079 nm) and Cu (0.3615 nm). This report is the first describing that shells can be overgrown epitaxially on cores even in the presence of a large lattice mismatch of more than 10% in bimetallic core−shell nanocrystals. Since Cu shells of ≈30 nm in thickness are prepared as shown in Figure 3c and the lattice spacing between {111} facets is 0.208 nm, about 150 monolayers of Cu{111} shells are overgrown on the {111} facets of Au cores.

As described above, a triangular platelike Cu shell is grown epitaxially over Au cores. To examine the effects of the shapes and positions of Au cores for the epitaxial growth of a Cu shell, HR-TEM images of Au@Cu nanocrystals were observed. Figure 4a-1 to e-1 shows HR-TEM images of octahedral, triangular and hexagonal platelike, decahedral, and icosahedral Au@Cu nanocrystals. In all particles, black contrast Au cores are covered by light contrast Cu shells. Parts a-2 to e-2, respectively, of Figure 4 show expanded

TEM images of the blue-circled parts of Figure 4a-1 to e-1. Further expanded HR-TEM images of Figure 4c-2 and e-2 are presented in Figures S1 and S2 in the Supporting Information. In all cases, fringes are observed on the flat facets of Cu, as shown in Figures S1 and S2 in the Supporting Information. The appearance of interference fringe patterns on the flat facets attests to the single-crystallinity of these copper shells. Fringes with spacing of 0.22 nm were assigned to the $3 \times \{422\}$ lattice spacing of the fcc copper crystal (e.g., the interval between the narrow red lines in Figure 4c-2 and Figure S1 in the Supporting Information).[22−24] The single-crystalline nature of the nanoplates was further confirmed by their electron diffraction patterns (Figure 3d), which show hexagonally arranged diffraction double spots with 6-fold symmetry characteristics of {111}-oriented single-crystal gold and copper nanoplates.

Previous studies of planar structures (such as thin films grown on various substrates) often revealed Moiré patterns in the TEM images.[25] Moiré patterns, which are arrays of parallel lines, were observed for octahedral, triangular, hexagonal platelike, and decahedral Au@Cu particles (Figure 4a-2 to d-2). However, no Moiré pattern was found for icosahedral Au@Cu particles (Figure 4e-2). The formation of these patterns is attributable to the difference in the plane interval between the gold core and copper shell nanoplates. For the array of parallel lines of Cu and Au lines with a $3 \times \{422\}$ lattice spacing of 0.222 nm (p_1) for Cu and 0.250 nm (p_2) for Cu, the interval of the Moiré pattern, λ, is calculated as 1.93 nm from the relation $\lambda = 2p_1p_2/(p_1 - p_2)$.[25] The observed interval 1.87 ± 0.18 nm in Figure 4c-2 shows reasonable agreement with the calculated value. This finding also supports the occurrence of epitaxial growth of the {111} plane of Cu over that of Au in many cases.

The HR-TEM (Figure 4) and TEM-EDS (Figure 2) data indicate that the degree of epitaxial growth of Cu shells depends on the shape and position of the Au cores. Octahedral and triangular Au cores are reserved well in Cu shells, although few Cu shells are grown on the corners, as indicated by red arrows in Figure 4a-3 and b-3). In the cases of hexagonal platelike and decahedral Au@Cu particles, there are more corners (Figure 4c-3 and d-3), so that shapes of Cu shells are reserved to a lesser extent than those for octahedral and triangular platelike Au@Cu nanocrystals. In cases of icosahedral particles with 12 pentagonal corners (Figure 4e-3), only asymmetric spherical Cu shells are grown over Au cores (Figure 4e-1), although Cu fringes were also observed in the contact area between Au and Cu facets (Figure S2), which implies that the epitaxial growth can occur on the contact area between Au core and Cu shell layers, although the icosahedral shape of the Au core is not well reserved in Cu shells. Summarizing the findings presented above, the degrees of epitaxial growth of Cu shells over Au cores were of the following order: octahedron and triangular-plate > hexagonal-plate and decahedron > icasahedron.

Growth Mechanisms of Au@Cu Nanocrystals. Fan et al.[7] pointed out three important factors for the epitaxial layered growth of heterogeneous core−shell nanocrystals: (i) lattice constants, (ii) electronegativity, and (iii) bond energy, as described in the Introduction. For Au@Cu particles, rule i does not hold because of a large lattice mismatch (11.4%). According to rule ii, the electronegativity of the shell metal should be lower than that of the core metal to avoid the displacement reaction and to wet the surface of the core easily. The standard electrode potential of Cu^{2+}/Cu^0 (+0.34 eV vs NHE) is lower than that of Au^{3+}/Au^0 (1.52 eV). Therefore, rule ii holds for Au@Cu particles. Rule iii necessitates that the bond energy between metal atoms of the shell be smaller than that between the shell atoms and substrate atoms to ensure growth in the Frank−van der Merwe mode. Actually, the bond energy of Cu−Cu (201.7 ± 0.4 kJ mol^{-1}) is less than that of Au−Cu (235.6 ± 9.2 kJ mol^{-1}),[26] showing that this rule also holds for Au@Cu particles. Consequently, two of three rules hold in the present Au core Cu shell system, which implies that only the effects of lattice mismatch can be examined for the epitaxial growth in Au@Cu nanocrystals.

When Cu nanoparticles were prepared using the same Cu salt in EG under oil-bath heating and MW heating, only spherical Cu nanoparticles were obtained (Figure S3 in Supporting Information). No well-defined single crystals, or single-twin and multiple-twin nanocrystals were prepared. Nevertheless, we were able to synthesize Cu nanocrystals having well-defined facets in the presence of Au cores as Cu shells. In many cases, the shapes of the Au cores are either reserved well or partially reserved, leading us to conclude that the mismatch of two metals (11.4%) is not a significant factor for the epitaxial growth of Cu over Au. We compared the epitaxial growth of Au@Cu nanocrystals from various Au core nanocrystals. The degree of epitaxial growth of Au@Cu nanocrystals depends strongly on the shape and position of Au cores. No twin plate exists for single-crystal octahedral particles, although triangular and hexagonal plates and decahedral and icosahedral particles have 1, 5, and 30 twin planes, as shown by the red lines in Figure 4b-3 to e-3. Epitaxial growth of the octahedral Cu shell is more favorable than that of the other single-twin and multiple-twin particles, if the presence of a twin plane suppresses the epitaxial growth of the Cu shell. We found here that the epitaxial growth on flat {111} facets occurs for all particles. However, epitaxial growth of the Cu shell on sharp corners is much slower than that on flat planes, irrespective of the presence and number of twin planes. Consequently, the epitaxial growth rate of the corners of octahedral particles is also slow. To form Cu epitaxial layers on octahedral, triangular-plate, hexagonal-plate, decahedral, and icosahedral particles on the sharp corners, four or five neighboring facets must be mutually matched in every layer, as shown by red arrows and the numbers 4 and 5 shown in Figure 4a-3 to e-3. Because a large mismatch exists in the lattice constant between Au and Cu (11.4%), Cu shells have some distortion. Such a distortion of Cu shell layers suppresses the epitaxial growth rate of the Cu shell, especially on the corners. Decahedral and icosahedral particles consist of tetrahedral units.[27] However, these crystals have some defects, as shown in Figure 5. Although no cavities attributable to such defects are observed in the products, decahedral and icosahedral Au particles have some defects in their crystals, especially in edge parts. Such defects constitute another reason why epitaxial growth of perfect shapes of Cu shells is more difficult than that in octahedral and triangular and hexagonal platelike particles, which have no such defects.

The results of this study show that the degree of epitaxial growth of Au@Cu nanocrystals depends strongly on the shape and position of Au cores. The epitaxial growth rate is especially slow on the corners of cores. On the other hand, such a great reduction of epitaxial growth rate on the corners of cores has not been observed for Au@Ag (lattice mismatch

0.2%), Pt@Pd (0.77%), or Au@Pd (4.7%), having smaller lattice mismatches.[4−9,18−20] That apparent lack of reduction for these three core−shell nanocrystals implies that the degree of epitaxial growth on the corners of cores depends on lattice mismatch between core and shell metals and that a small lattice mismatch is required for the epitaxial growth of shells on the sharp corners.

Particles. The Cu nanoparticles are known to be oxidized easily to Cu_2O after leaving Cu particles in the presence of residual O_2 dissolved in solutions.[28,29] To examine the content of O atoms after leaving Au@Cu particles in a glass bottle for more than 1 day, TEM−EDS data for Au, Cu, and O atoms were measured. Typical TEM, TEM−EDS, and line analysis data are shown in Figure S4 (Supporting Information). We found that a very small amount of O component is distributed uniformly at the same position of Cu shells. For example, the atomic ratios of Au/Cu/O within the blue circle in Figure S4 were 13.32:86.34:0.34%, respectively, showing that very thin oxide layers are formed uniformly. The Cu_2O layers are formed when a solution of Au@Cu particles is left in a glass bottle. In addition, a high probability exists that Cu_2O layers are produced either during the washing step required to remove the excess PVP (which interferes with TEM characterization) or during drying of the colloid on the TEM grid. Pastoriza-Santos et al. observed diffraction spots and thin layers of Cu_2O in SAED and HR-TEM measurements of Cu nanoplates.[29] However, we could not detect diffraction spots and layers of Cu_2O for Au@Cu particles in the present measurements due to a very low content of O atom. When XPS of Au@Cu particles was measured 4 days after preparation, little peak of O 1s from Cu_2O was observed at 530.2 eV.[30] These findings imply that the Cu_2O layer was too thin to be detected by SAED, HR-TEM, and XPS.

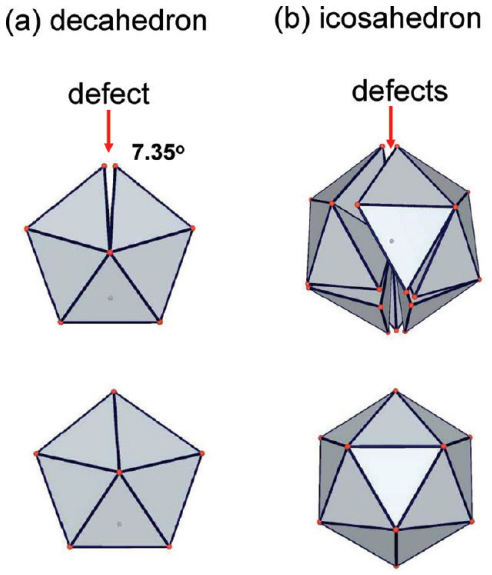

Figure 5. Decahedral and icosahedral particles formed by combination of tetrahedral units.

In general, oxidation of Cu nanoparticles gave rise to a progressive damping of the surface plasmon band (SPR) because of growth of the oxide outer shell.[13,28,29] Consequently, the extent of oxidation of Cu nanoparticles can be examined by observing the intensity change in the SPR band at ≈600 nm. The UV−vis−NIR spectra were measured to characterize optical properties and to elucidate the time evolution and antioxidative properties of Au@Cu particles (Figure 6a). For comparison, UV−vis−NIR spectra of typical spherical Cu particles in EG are also shown in Figure 6b. In Figure 6a, the SPR band of Au core particles with a peak at ≈570 nm is observed in the 250−1000 nm region. After heating for 5−15 min, a peak of an SPR band with a peak at ≈610 nm appears; its intensity increases during 5−10 min. The SPR peak at 15 min resembles that at 10 min, indicating that the reduction of Cu was completed at 10 min, immediately after the end of the injection of the Cu reagent. The peak position at 610 nm agrees well with that of Cu particles (Figure 6b), showing that Au@Cu particles have optical properties of Cu shells. When a solution is left in air for 1 day or 1 week, the SPR band intensity decreases by 9% or 20%. On the other hand, a weak SPR band with a peak ≈600 nm was observed in the 250−1000 nm region for monometallic Cu particles (Figure 6b). This band can be ascribed to the SPR band of Cu nanoparticles.[13,28,29] It is noteworthy that the peak intensity of the SPR band of Cu decreases by 17% or 67% after 1 day or 1 week. The slight red-shifting and broadening of the SPR bands of Au@Cu particles in comparison with those of the pure Cu particles (Figure 6b) arises from large particle sizes, their wide size distributions, and a change in the dielectric constant of Cu by the presence of Au cores. The slow diminution of the SPR peaks suggests that Au@Cu particles have a higher antioxidative property than those of pure Cu particles. Similar antioxidative properties

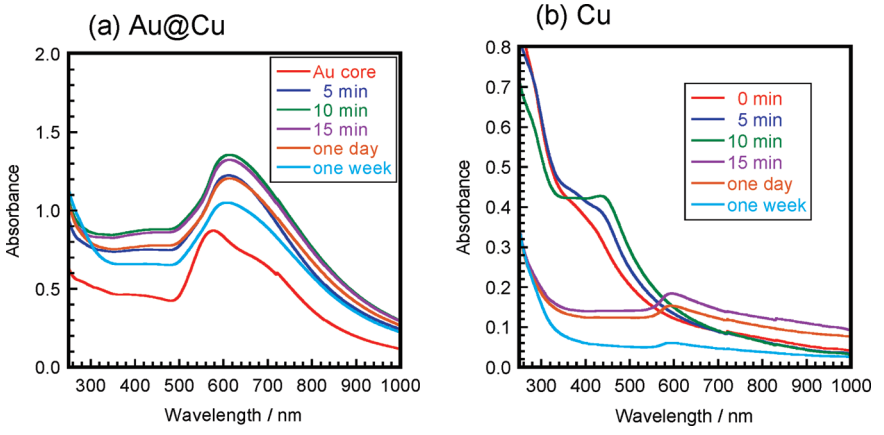

Figure 6. (a) Time dependence of UV−vis−NIR spectra of Au@Cu and (b) Cu nanoparticles prepared using the polyol method.

by the presence of core particles have been observed for Ag@Cu and Ag/Cu alloy core Cu shell particles.[31,32] The electron affinity of Au (2.309 eV) is greater than that of Cu (1.228 eV). Consequently, electrons in Cu shells are drawn by Au cores. Therefore, when O_2 attaches to the Cu surface to form Cu_2O, a lower density of electrons in Cu can be supplied to O atom in the presence of Au cores. This is the main reason for the appearance of the highly antioxidative properties in Au@Cu particles.

Conclusion

The lattice mismatch between cores and shells has been believed to be less than 5% for the epitaxial growth of shells over cores in bimetallic nanoparticles. Our present results show that the epitaxial layered growth of Cu shells over polygonal Au cores rarely occurs despite a lattice mismatch of Au and Cu as great as 11.4%. This implies that an exceptional case exists in which epitaxial growth occurs even with a large lattice mismatch greater than 10%. The favorable facets of the Cu shell were {111}, which were the same as the major facets of the Au core seeds. The SAED patterns and appearance of Moiré patterns indicated that single crystals of Cu layers formed parallel to those of Au seeds. The growth rates of Cu shells on sharp corners of Au cores were slower than those on flat {111} facets and single twin facets. This was explained by the facts that matching of more than four facets is necessary for the sharp corners and that distortion exists in decahedral and icosahedral crystals. The Au@Cu nanoparticles showed a higher antioxidative property than that of pure Cu particles prepared under identical conditions. That property was explained by larger electron drawing effects of Au than those of Cu, which suppress Cu_2O formation.

Acknowledgment. We thank Mrs. S. Hikino for her assistance in the preparation of Cu nanoparticles using a polyol method and Prof. J. Yamaki and Mr. E. Kobayashi for the XPS measurements. This work was supported by a Grant-in-Aid for Scientific Research (B) from the Ministry of Education, Culture, Sports, Science, and Technology of Japan (MEXT, No. 22310060) and by the Management Expenses Grants for National Universities Corporations from the MEXT.

Supporting Information Available: Expanded HR-TEM images of Au@Cu nanocrystals, TEM image of a Cu nanoparticle prepared by the polyol method, and TEM-EDS data involving the O component. This material is available free of charge via the Internet at http://pubs.acs.org.

References

(1) Toshima, N. *Pure Appl. Chem.* **2000**, *72*, 317.
(2) Hodak, J.; Henglein, A.; Giersig, M.; Hartland, G. V. *J. Phys. Chem. B* **2000**, *104*, 11708.
(3) Nadagouda, M. N.; Varma, R. S. *Cryst. Growth Des.* **2007**, *7*, 2582.
(4) Xiang, Y.; Wu, X.; Liu, D.; Jiang, X.; Chu, W.; Li, X.; Ma, Y.; Zhou, W.; Xie, S. *Nano Lett.* **2006**, *6*, 2290.
(5) Xue, C.; Millstone, J. E.; Li, S.; Mirkin, C. A. *Angew. Chem., Int. Ed.* **2007**, *46*, 8436.
(6) Habas, S. E.; Lee, H.; Radmilovic, V.; Somorjai, G. A.; Yang, P. *Nat. Mater.* **2007**, *6*, 692.
(7) Fan, F.-R.; Liu, D.-Y.; Wu, Y.-F.; Duan, S.; Xie, Z.-X.; Jiang, Z.-Y.; Tain, Z.-Q. *J. Am. Chem. Soc.* **2008**, *130*, 6949.
(8) Wu, Y.; Jiang, P.; Jiang, M.; Wang, T,-W.; Guo, C.-F.; Xie, S.-S.; Wang, Z.-L. *Nanotechnology* **2009**, *20*, 305602 (10 pp).
(9) Lee, Y. W.; Kim, M.; Kim, Z. H.; Han, S. W. *J. Am. Chem. Soc.* **2009**, *131*, 17036.
(10) Zhang, H. T.; Ding, J.; Chow, G. M.; Ran, M.; Yi, J. B. *Chem. Mater.* **2009**, *21*, 5222.
(11) (a) Hu, J.-W.; Li, J.-F.; Ren, B.; Wu, D.-Y.; Sun, S.-G.; Tian, Z.-Q. *J. Phys. Chem. C* **2007**, *111*, 1105. (b) Deng, S.; Pingali, K. C.; Rockstraw, D. A. *IEEE Sens. J.* **2008**, *8*, 730. (c) Yang, Y.; Shi, J.; Kawamura, G.; Nogami, M. *Scr. Mater.* **2008**, *58*, 862.
(12) Majo, K. J.; De, C.; Obare, S. O. *Plasmonics* **2009**, *4*, 61.
(13) (a) Tsuji, M.; Hikino, S.; Sano, Y.; Horigome, M. *Chem. Lett.* **2009**, *38*, 518. (b) Tsuji, M.; Hikino, S.; Tanabe, R.; Sano, Y. *Chem. Lett.* **2009**, *38*, 860. (c) Tsuji, M.; Hikino, S.; Tanabe, R.; Yamaguchi, D. *Chem. Lett.* **2010**, *39*, 334.
(14) Tsuji, M. Core Shell Particles. In *Shape and Structure Control of Metal Nano- and Fine-particles*; Yonezawa, T., Ed.; CMC: Tokyo, 2009; p 166 (in Japanese).
(15) Sobal, N. S.; Ebels, U.; Möhwald, H.; Giersig, M. *J. Phys. Chem. B* **2003**, *107*, 7351.
(16) Yan, J.-M.; Zhang, X.-B.; Akita, T.; Haruta, M.; Xu, Q. *J. Am. Chem. Soc.* **2010**, *132*, 5326.
(17) Sobal, N. S.; Hilgendorff, M.; Möhwald, H.; Giersig, M.; Spasova, M.; Radetic, T.; Farle, M. *Nano Lett.* **2002**, *2*, 621.
(18) Tsuji, M.; Miyamae, N.; Lim, S.; Kimura, K.; Zhang, X.; Hikino, S.; Nishio, M. *Cryst. Growth Des.* **2006**, *6*, 1801.
(19) (a) Tsuji, M.; Matsuo, R.; Jiang, P.; Miyamae, N.; Ueyama, D.; Nishio, N.; Hikino, S.; Kumagae, H.; Kamarudin, K. S. N.; Tang, X.-L. *Cryst. Growth Des.* **2008**, *8*, 2528. (b) Tsuji, M.; Ogino, M.; Matsunaga, M.; Miyamae, N.; Matsuo, R.; Nishio, M.; Alam, M. J. *Cryst. Growth Des.* **2010**, *10*, 4085.
(20) Tsuji, M.; Nishio, M.; Jiang, P.; Miyamae, N.; Lim, S.; Matsumoto, K.; Ueyama, D.; Tang, X. *Colloids Surf., A* **2008**, *317*, 247.
(21) (a) Tsuji, M.; Hashimoto; Nishizawa, Y.; Tsuji, T. *Chem. Lett.* **2003**, *32*, 1114. (b) Tsuji, M.; Hashimoto, M.; Nishizawa, Y.; Kubokawa, M.; Tsuji, T. *Chem.—Eur. J.* **2005**, *11*, 440. (c) Tsuji, M.; Miyamae, N.; Hashimoto, M.; Nishio, M.; Hikino, S.; Ishigami, N.; Tanaka, I. *Colloids Surf., A* **2007**, *302*, 587. (d) Tsuji, M.; Miyamae, N.; Nishio, M.; Hikino, S.; Ishigami, N. *Bull. Chem. Soc. Jpn.* **2007**, *80*, 2024.
(22) Germain, V.; Li, J.; Ingert, D.; Wang, Z. L.; Pileni, M. P. *J. Phys. Chem. B* **2003**, *107*, 8717.
(23) Rodríguez-González, B.; Pastoriza-Santos, I.; Liz-Marzán, L. M. *J. Phys. Chem. B* **2006**, *110*, 11796.
(24) Xie, J.; Lee, J. Y.; Wang, D. I. C. *J. Phys. Chem. C* **2007**, *111*, 10226.
(25) Williams, D. B.; Carter, C. B. *Transmission Electron Microscopy: A Textbook for Materials Science*, 2nd ed.; Springer: 2009.
(26) David, R. L. *CRC Handbook of Chemistry and Physics*, Internet Version 2007, 87th ed.; Taylor and Francis: Boca Raton, FL.
(27) Tsuji, M.; Ogino, M.; Matsuo, R.; Kumagae, H.; Hikino, S.; Kim, T.; Yoon, S.-H. *Cryst. Growth Des.* **2010**, *10*, 296.
(28) Kanninen, P.; Johans, C.; Merta, J.; Kontturi, K. *J. Colloid Interface Sci.* **2008**, *318*, 88.
(29) Pastoriza-Santos, I.; Sánchez-Iglesias, A.; Benito Rodríguez-González, B.; Liz-Marzán, L. M. *Small* **2009**, *5*, 440.
(30) (a) Panzner, G.; Egert, B.; Schmidt, H. P. *Surf. Sci.* **1985**, *151*, 400. (b) Ghijsen, J.; Tjeng, L. H.; van Elp, J.; Eskes, H.; Westerink, J.; Sawatzky, G. A.; Czyzyk, M. T. *Phys. Rev. B* **1988**, *38*, 11322.
(31) Nakamura, T.; Tsukahara, Y.; Yamauchi, T.; Sakata, T.; Mori, H.; Wada, Y. *Chem. Lett.* **2007**, *36*, 154.
(32) Tsuji, M.; Hikino, S.; Tanabe, R.; Matsunaga, M.; Sano, Y. *CrystEngComm* **2010**, *12*, 3900.